

IR820-loaded PLGA nanoparticles for photothermal therapy of triple-negative breast cancer

Danielle M. Valcourt,¹ Megan N. Dang,¹ Emily S. Day^{1,2,3}

¹Department of Biomedical Engineering, University of Delaware, 161 Colburn Lab, Newark, Delaware, 19716

²Department of Materials Science & Engineering, University of Delaware, 201 DuPont Hall, Newark, Delaware, 19716

³Helen F. Graham Cancer Center & Research Institute, 4701 Ogletown Stanton Road, Newark, Delaware, 19713

Received 23 October 2018; revised 25 February 2019; accepted 22 March 2019

Published online 00 Month 2019 in Wiley Online Library (wileyonlinelibrary.com). DOI: 10.1002/jbm.a.36685

Abstract: Triple-negative breast cancer (TNBC) accounts for 15–25% of breast cancer cases and lacks expression of the three most common receptors seen on other subtypes of breast cancer. This lack of expression makes TNBC unsusceptible to currently available targeted or hormonal therapies, so new treatment strategies are desperately needed. Photothermal therapy (PTT), which utilizes nanoparticles (NPs) embedded in tumors as exogenous energy absorbers to convert externally applied near-infrared (NIR) light into heat to ablate cancer cells, has shown promise as an alternative strategy. However, it typically uses gold-based NPs that will remain in the body for extended period of time with unknown long-term health effects. To enable PTT

with biodegradable, polymeric NPs, we encapsulated the NIR-absorbing dye IR820 in poly(lactic-co-glycolic acid) (PLGA) NPs. We characterized the physicochemical properties of these IR820-loaded PLGA NPs and evaluated their performance as PTT agents using both *in vitro* and *in vivo* models of TNBC. The results demonstrate that these NPs are potent mediators of PTT that induce cell death primarily through apoptosis to effectively hinder the growth of TNBC tumors. © 2019 Wiley Periodicals, Inc. *J Biomed Mater Res Part A*: 00A: 000–000, 2019.

Key Words: hyperthermia, polymer nanoparticle, near-infrared light, cancer nanomedicine, apoptosis

How to cite this article: Valcourt DM, Dang MN, Day ES. 2019. IR820-loaded PLGA nanoparticles for photothermal therapy of triple-negative breast cancer. *J Biomed Mater Res Part A* 2019;9999A:1–11.

INTRODUCTION

Triple-negative breast cancer (TNBC) accounts for 15–25% of all breast cancer cases and it lacks expression of the three most common receptors found on other subtypes of breast cancer: estrogen receptor, progesterone receptor, and human epidermal growth factor receptor 2.^{1,2} This lack of expression makes TNBC unsusceptible to current targeted or hormonal therapies and results in high recurrence and mortality rates.^{1–3} Several alternative treatment strategies have shown promise against TNBC, including photothermal therapy (PTT),^{4–7} which utilizes nanoparticles (NPs) embedded in tumors as exogenous energy absorbers to convert externally applied near-infrared (NIR) light into heat to ablate cancer cells.^{8–10} In NP-mediated PTT, NPs delivered systemically accumulate in tumors through their leaky vasculature,^{11,12} and are then irradiated with NIR light, which causes them to produce heat sufficient to induce tumor cell death.^{10,13} The use of NIR light is important for PTT because NIR light can penetrate deeper into tissue than visible wavelengths since it is minimally absorbed by the major components of tissue it will encounter prior to reaching the diseased site.^{9,10,14–16} The key advantages of PTT are that it is simple to perform, it

enables high precision since heat is generated only where NPs and light are combined, and it is less susceptible to cellular resistance because it induces cell death through physical mechanisms such as membrane rupture and protein denaturation.¹⁰ Additionally, the mechanism of cell death can be tuned between apoptosis and necrosis by controlling treatment parameters such as the type of NP used and the irradiation conditions.⁸ This is elaborated upon below, and is important since the mechanism of cell death can influence overall treatment success when PTT is applied alone or in combination settings. Here, we aimed to develop biodegradable, polymeric NPs to mediate proapoptotic PTT of TNBC as a standalone therapy.

As just introduced, the mechanism of cell death induced by PTT plays a critical role in treatment success. Typically, PTT has been applied in a manner that yields rapid and very high heating that causes cellular necrosis. However, when cells undergo necrosis, there is a pro-inflammatory response that can elicit a negative immune reaction, which may actually promote tumor recurrence.^{8,17,18} It is critical to produce immunogenic cell death, which is largely temperature dependent, to achieve long-term survival.¹⁹ Thus, applying mild

Additional Supporting Information may be found in the online version of this article.

Correspondence to: E. S. Day; e-mail: emilyday@udel.edu

Contract grant sponsor: National Institute of General Medical Sciences; contract grant numbers: P20GM103446 and R35GM119659

Contract grant sponsor: National Science Foundation; contract grant numbers: IIA-1301765

hyperthermia to induce apoptosis rather than necrosis may be preferable when PTT is applied as a standalone therapy because apoptosis is anti-inflammatory and can promote a positive immune response that enhances tumor regression and long-term remission.^{8,20} However, there are instances where necrosis may be the preferred mechanism of cell death, such as when PTT is combined with immunotherapy. This is because PTT that induces necrosis can release damage-associated molecular patterns and tumor-associated antigens that may engage a tumor-specific immune response to potentiate immunotherapy.^{21,22} Bear et al. demonstrated that the pro-inflammatory cytokines and chemokines released during PTT-induced necrosis could promote the maturation of dendritic cells in tumor-draining lymph nodes.¹⁸ However, they found this does not contribute to overall antitumor immunity and may even promote the growth of distant metastases unless combined with a form of immunotherapy, in this case adoptive T cell transfer.¹⁸ Chen et al. similarly found that combining indocyanine green-mediated PTT with an immune adjuvant Imiquimod R837 could generate a vaccine-like function in mice bearing 4T1 TNBC tumors.²¹ These examples demonstrate the importance of understanding the fundamental mechanism of cell death induced by PTT, and the need to tailor the mechanism based on the specific application and whether PTT is applied as a standalone or combination therapy.

Since the mechanism of cell death is influenced by the level of tumor heating achieved during treatment, it is important to note that there are several parameters that influence heat production in NP-mediated PTT, including the photothermal conversion efficiency of the NPs, the energy of irradiation applied, the density of the surrounding tissue, and even the localization of the NPs within the target cells and tissue.^{23,24} For example, apoptosis can be achieved as the primary mechanism of cell death by using lower energy irradiation.^{8,25-27} To control NP localization in the tumor microenvironment, targeting agents could be incorporated into the NP design, but there is currently substantial debate surrounding the benefit provided by this strategy, as targeted NPs may not offer a dramatic benefit compared to NPs that rely on strictly passive tumor accumulation.²⁸ Finally, heat production during PTT could be altered by using NPs with different photothermal conversion efficiencies. Historically, photothermally active NPs used for PTT have been gold-based because they offer high photothermal conversion efficiencies as well as ease of synthesis and surface modification.^{10,29-32} Nanoshells, in particular, are currently being investigated in clinical trials to mediate PTT of head and neck tumors and prostate tumors.³³⁻³⁵ However, gold-based NPs will remain in the body for extended period of time with unknown long-term health effects.¹⁰ To prevent possible long-term health effects associated with nondegradable NPs, researchers have begun to develop organic, nongold-based photothermal agents.³⁶ By incorporating NIR-absorbing dyes into biodegradable platforms, these nanocarriers can facilitate photothermal ablation of tumors, while also providing dual-imaging capabilities.³⁷⁻⁴⁵

Some examples of organic PTT agents reported in the literature include micelles⁴⁶ and lipid-based bilayers,⁴⁷ as well

as more complex polymer blends⁴⁸ and conjugates.³⁷ Peng et al. have loaded micelles with IR780 dye and labeled these NPs with radionuclide rhenium-188 to further enhance their imaging capabilities.⁴⁶ Lovell et al. have developed unique NPs designated as porphosomes, which are a self-assembled bilayer of porphyrin that can provide PTT following irradiation with 660 nm light without loading any additional photothermal agents.⁴⁷ In addition, Yue et al. have created IR780-loaded heparin-folic acid conjugates for targeted imaging and photothermal ablation of MCF-7 xenograft tumors.³⁷ While these and other organic NP platforms show great promise in treating primary tumors, few studies have examined the mechanism of cell death induced by PTT with these agents, which is critical to maximize treatment success. One such study, conducted by Li et al., used a terminal deoxynucleotidyl transferase dUTP nick end labeling assay on tumors excised after treatment to show that their full NP formulation (docetaxel and IR820 coloaded micelles functionalized with Lyp-1 peptides) could induce apoptosis in tumors in mice leading to remission.⁴⁹ This was an exciting finding, but the complexity of this NP formulation may pose a significant barrier to its clinical translation.⁵⁰ Similarly, Zheng et al. developed polymer NPs encapsulating both doxorubicin and indocyanine green and evaluated their impact on cellular apoptosis and necrosis postirradiation *in vitro* using an Annexin V/propidium iodide (PI) assay.⁵¹ They found that PTT mediated by their NPs induced a substantial amount of cell death, but the amount of cell death was only ~10% greater than that induced by the NPs without light irradiation, which provide strictly doxorubicin delivery. Further, of this additional cell death, >33% was necrotic, rather than apoptotic,⁵¹ suggesting there is still more for the field to learn regarding designing biodegradable NPs to maximize apoptosis upon PTT. Overall, these prior studies and others demonstrate that organic PTT agents are an attractive alternative to gold-based NPs that can yield potent antitumor effects.^{21,48,49,51}

In this work, we have developed biodegradable, polymeric NPs comprised of poly(lactic-co-glycolic acid) (PLGA) loaded with the NIR-absorbing dye IR820 (IR820-PLGA NPs) to enable proapoptotic PTT of TNBC. These NPs eliminate the health concerns associated with gold-based NPs and are capable of dual imaging and therapy since IR820 not only heats, but also emits fluorescence at 820 nm upon excitation with 710 nm light, which overlaps with the first characteristic extinction peak of the dye. The ability to image these NPs can inform therapy by indicating when the NPs have maximally accumulated within tumors, marking the optimal time for laser application. We also demonstrate that PTT mediated by these NPs, under the laser irradiation conditions utilized here, induces cell death primarily through apoptosis rather than necrosis, which is important given the above discussion regarding the consequences this may have on tumor recurrence and metastasis. Overall, this work demonstrates the utility of IR820-PLGA NPs as potent mediators of proapoptotic PTT both *in vitro* and *in vivo*, warranting further investigation of their use to treat TNBC and other forms of cancer that lack effective treatment strategies.

MATERIALS AND METHODS

Synthesis of IR820-PLGA NPs

IR820-PLGA NPs were synthesized using the well-established single emulsion method.⁵² Briefly, PLGA (LACTEL, 50:50 carboxylic acid terminated) was dissolved in acetone (VWR) at 1 mg/mL. IR820 dye (Sigma, stored in methanol at 0.5 g/mL) was added to the PLGA in acetone solution at a concentration of 0.5 mg/mL, and this mixture was subsequently added dropwise to distilled water in a 1:3 volume ratio while stirring. This emulsion continued to stir for 2 h, letting the acetone evaporate. The NPs were then purified using centrifugal filtration (Millipore, 10 k MWCO, 4200 g, 30 min) to remove unencapsulated IR820 and excess solvent.

Characterization and stability of IR820-PLGA NPs

The purified NPs were characterized by dynamic light scattering (DLS) and zeta potential measurements on a Litesizer500 instrument (Anton Paar), and the reported intensity-based hydrodynamic diameter is the z-average of three measurements. DLS measurements of hydrodynamic diameter and polydispersity index, which is an output of the equipment, were taken every 2 days for 1 month to demonstrate the NPs' stability in storage conditions (4 °C in water). The data shown are the average of three trials and error bars represent standard deviations. IR820-PLGA NP samples for transmission electron microscopy (TEM) were prepared on 400 mesh carbon-coated copper grids that were rendered hydrophilic in a PELCO easiGlow glow discharge unit. The freshly glow discharged grids were floated on drops of the sample for several seconds, washed with nanopure water, and negatively stained with 2% uranyl acetate. After drying, the grids were imaged (Gatan UltraScan 1000 CCD camera) on a Zeiss LIBRA 120 TEM operating at 120 kV.

IR820 encapsulation in NPs was characterized by ultraviolet-visible (UV-vis) spectroscopy (Cary 60 spectrophotometer, Agilent) based on reading the absorbance of the NPs at 810 nm and comparing to a standard curve of known dye concentration. The samples were scanned from 400 to 1100 nm with baseline correction at a scan rate of 2400 nm/s. The amount of IR820 released from the NPs while in storage conditions was also examined by UV-vis spectroscopy. At several time points between 0 and 30 days postpreparation, NP samples were centrifuge filtered to separate the NPs from released IR820, and the collected released IR820 was compared to a standard curve of known dye concentration using the same scanning conditions as described above. Studies to analyze IR820 release in storage conditions were performed three times and the data shown are the average and standard deviation of all three trials.

The heating profile of free IR820 and IR820-PLGA NPs was measured upon laser excitation with thermal camera imaging (FLIR A5). Samples were suspended in phosphate buffered saline (PBS) at an IR820 concentration of 25 μ M and incubated at 37 °C prior to laser irradiation. The free dye and NP samples were then irradiated with a continuous wave 808 nm laser (B&W Tek) for 5 min at 1.5 W/cm². The concentration dependence of the heating profile for IR820-PLGA NPs was examined by irradiating IR820-PLGA NPs at concentrations of 10, 25, or

35 μ M IR820 with the 808 nm laser set to 1.5 W/cm² for 5 min. The dependence of heating on laser intensity was similarly evaluated by irradiating IR820-PLGA NPs suspended in PBS at 25 μ M with the 808 nm laser set to 0.5, 1, 1.5, 2, or 3 W/cm² for 5 min. The temperature in each sample was recorded once every minute during irradiation and experiments were repeated three times. To understand the influence of heating on the optical and physical properties of the NPs, the absorbance spectra, hydrodynamic diameter, and polydispersity index of IR820-PLGA NPs stored in PBS at 25 μ M were recorded by UV-vis spectroscopy and DLS both before and after irradiation of samples with the 808 nm laser at 1.5 W/cm² for 5 min. Hydrodynamic diameter and polydispersity index data shown are an average of three measurements taken before and after irradiation. Error bars represent standard deviation.

Cell culture

MDA-MB-231 TNBC cells (ATCC) were cultured in Dulbecco's Modified Eagle's Medium (VWR) supplemented with 10% fetal bovine serum (Gemini Bio Products) and 1% penicillin-streptomycin (VWR). The culture was maintained at 37 °C in a 5% CO₂ humidified environment. When cells reached 80–90% confluency in T75 cell culture flasks, they were passaged or plated by detaching the cells from the flask using Trypsin-EDTA (Thermo Fisher) and then counting the cells with a hemocytometer.

Cellular binding and uptake of free IR820 and IR820-PLGA NPs

To analyze cellular binding and uptake of free IR820 dye and IR820-PLGA NPs by flow cytometry, cells were plated at 1×10^5 cells per well in 24-well plates and incubated overnight. Cells were then treated with 0, 10, 25, or 35 μ M free IR820 dye or IR820-PLGA NPs (prepared as described above) and incubated for 4 h to evaluate dose dependency. To prepare the free IR820 samples, IR820 stored in methanol at 0.5 g/mL was first diluted in PBS to 350 μ M and then added to the cell culture media to yield these respective concentrations. After 4 h, the cells were rinsed with PBS, lifted off the plate with Trypsin-EDTA, and resuspended in PBS to yield a single cell suspension for analysis of uptake by flow cytometry using an Acea NovoCyte 2060 Flow Cytometry. To evaluate time dependency, cells were treated with 35 μ M free IR820 dye or IR820-PLGA NPs for 0, 2, 4, 6, or 8 h prior to rinsing with PBS. The cells were then lifted off the plate with Trypsin-EDTA and resuspended in PBS to yield a single cell suspension. All cell suspensions were analyzed using an Acea NovoCyte 2060 Flow Cytometry with the APC-Cy7 (excitation, 640 nm; emission, 780/60 nm) channel. Density plots showing forward and side scatter data were used to create a primary gate for cells, excluding debris, prior to analyzing IR820 content.

Effect of free IR820 and IR820-PLGA NPs on metabolic activity

To evaluate the toxicity of free IR820 and IR820-PLGA NPs in the dark using a 3-(4,5-dimethylthiazol-2-yl)-2,5-diphenyltetrazolium bromide (MTT) assay, cells were seeded in a 96-well plate at

1×10^4 cells per well and incubated overnight. Cells were treated with 0, 5, 10, 15, 25, or 35 μM of free IR820 dye or IR820-PLGA NPs for 4 h. Then, the cells were washed with PBS and incubated in fresh media for an additional 24 h prior to being incubated in MTT solution per the manufacturer's instructions (Thermo Fisher). After 3 h, the MTT solution was replaced with dimethyl sulfoxide (DMSO) and the absorbance at 540 nm was read on a Synergy H1 plate reader (BioTek). To analyze the data, background (DMSO in wells without cells) was subtracted from the absorbance reading in each well. Triplicate well signals were averaged and then normalized to untreated cells. These experiments were performed in triplicate and analyzed by Student's *t* tests at each concentration.

Assessing metabolic activity following PTT

Cells were seeded as described above and treated with IR820-PLGA NPs at 35 μM or with fresh media (no treatment control) for 4 h while incubating at 37 °C. The cells were then washed with PBS and incubated in fresh media for 30 min to bring the temperature to 37 °C. Cells were then irradiated with the 808 nm continuous wave laser at 1.5 W/cm² for 5 min/well. The irradiation was performed at room temperature, with samples returned to the 37 °C incubator immediately following irradiation. After 24 h, an MTT assay was performed as described above. Data shown are from three experiments that were each run with triplicate wells and the data was analyzed by one-way ANOVA with post hoc Tukey.

Evaluating the mechanism of cell death induced by PTT

To analyze the mechanism of cell death induced by PTT mediated by IR820-PLGA NPs, cells were seeded at 3×10^4 cells per well in a 24-well plate and incubated overnight. Cells were then treated with 0 or 10 μM IR820-PLGA NPs for 4 h, at which time the cells were rinsed with PBS and the wells replenished with fresh media. The appropriate wells were then irradiated with continuous wave 808 nm light at 2 W/cm² for 5 min/well such that the treatment groups included no treatment, IR820-PLGA NPs only, light only, or IR820-PLGA NPs + light (PTT). These experiments were performed on a digital dry block heater (VWR) to ensure the initial temperature of 37 °C was maintained in each well through all irradiation procedures, and the samples were returned to the incubator after irradiation. After 24 h, an Annexin V/PI stain (Cayman Chemicals) was conducted per the manufacturer's instructions. Briefly, cells were lifted from the plate with Trypsin-EDTA, washed with 1x binding buffer, and resuspended in 50 μL binding buffer containing 1:500 Annexin V and 1:1000 PI stains for 10 min in the dark. The samples were then diluted with 150 μL 1x binding buffer and analyzed on the Acea NovoCyte 2060 Flow Cytometry with FITC (excitation, 488 nm; emission, 530/30 nm) and PerCP (excitation, 488 nm; emission, 675/30 nm) channels. Data analysis was performed in NovoExpress software (ACEA Biosciences). Density plots showing forward and side scatter data were used to create a primary gate for cells, excluding debris, prior to establishing gates for Annexin V-positive and PI-positive cells. Positive stained gates were

based on unstained cells and single stained controls were used for compensation. The data presented are the average of three experiments and were analyzed by one-way ANOVA.

In vivo tumor model

Female nude mice around 5 weeks old were purchased from Charles River Laboratories. The Institutional Animal Care and Use Committee of the University of Delaware approved the procedures. MDA-MB-231 cells in matrigel (1×10^6 cells per 100 μL) were administered subcutaneously into the right flank of the mice and tumor growth was monitored at least 3x weekly thereafter with Vernier calipers. Treatments (100 μL of either saline, free IR820 dye at a concentration of 350 μM , or IR820-PLGA NPs at a concentration of 350 μM) were administered intravenously when tumors reached 5 mm in diameter. The treatment concentration of 350 μM was based on literature values for intravenously delivered NIR-absorbing dyes.^{6,21,51,53} A preliminary biodistribution study utilized four mice (two that received saline and two that received IR820-PLGA NPs), and a therapeutic efficacy study utilized 47 mice that were treated as follows: saline (eight mice), saline with NIR irradiation (seven mice), free IR820 dye (eight mice), free IR820 dye with NIR irradiation (eight mice), IR820-PLGA NPs (eight mice), and IR820-PLGA NPs with NIR irradiation (eight mice). Details of these studies are provided in the following sections.

Assessment of the biodistribution of IR820-PLGA NPs *in vivo*

Our previous experience has revealed that 24 h is typically the optimum time for laser irradiation following intravenous delivery of photothermally active NPs,^{14,15} as this is when NPs maximally accumulate in tumors relative to adjacent healthy tissue. To reveal whether 24 h is also when IR820-PLGA NPs display maximum tumor accumulation, during the therapeutic efficacy study, the mice that received 100 μL of IR820-PLGA NPs were imaged under isoflurane anesthesia with an IVIS Lumina Imaging System (PerkinElmer) both immediately and again every 24 h for 4 days to monitor IR820 signal in the tumors versus time using the ICG channel (excitation, 788 nm; emission, 813 nm). We did not analyze earlier time points because many of the NPs would likely still be in circulation prior to 24 h. The fluorescence intensity at each time point was measured in the ImageJ software after drawing a region of interest around the tumor, and the mean intensity at each time point was calculated. This confirmed 24 h was the time of maximum NP accumulation in tumors, so we performed a separate biodistribution study with a small number of mice (two that received saline, two that received IR820-PLGA NPs) to reveal the more complete biodistribution of IR820-PLGA NPs at this timepoint. Then, 24 h postintravenous injection of the saline or IR820-PLGA NPs, the mice were euthanized and their major organs (heart, brain, liver, lungs, kidneys, and spleen) and tumors excised for analysis of IR820 signal using the IVIS.

Evaluating the effect of PTT on TNBC tumor temperature and growth *in vivo*

Mice were injected with 100 μL of free IR820 dye (350 μM), IR820-PLGA NPs (350 μM), or saline when tumors reached

5 mm in diameter as described above (hereafter, this is referred to as day 0). After 24 h, half of the mice in each group were anesthetized with isoflurane and their tumors irradiated with a continuous wave LightForce FXi laser (LiteCure) at 1.5 W/cm^2 for 5 min using a band-pass filter at 810 nm. During irradiation, the temperature of the tumor in each mouse was measured every minute using an FLIR A5 thermal camera. The mean and standard deviation of the tumor temperature in each treatment group were calculated. Subsequently, all six groups of mice (saline \pm laser; free IR820 \pm laser; IR820-PLGA NPs \pm laser) received three additional rounds of treatment on days 7, 14, and 21 for a total of four treatments. The tumor length and width in each mouse were measured with Vernier calipers 3x per week for 1 month and tumor volume was calculated as $(\text{tumor length}) \times (\text{tumor width})^2/2$. These data were used to calculate the mean and standard error of tumor volume in each group, and statistical differences between groups were determined by two-way ANOVA with post hoc Tukey. On day 30, the mice were euthanized and the major organs (spleen, liver, kidneys, heart, lungs, and brain) and tumors were excised for histological analysis by hematoxylin and eosin (H&E) staining. The excised tissues were placed into embedding cassettes, rinsed once in 1x PBS, and then fixed in 4% paraformaldehyde at 4°C for 72 h. The tissues were then rinsed three times in 70% ethanol for 10 min each and stored in 70% ethanol until processing. The fixed tissues were processed and embedded with paraffin. Embedded tissues were cut into $5 \mu\text{m}$ slices and stained with H&E to

enable visualization of tissue structure. Briefly, the tissues were deparaffinized with xylene and rehydrated prior to hematoxylin staining and subsequent counterstaining with eosin. After staining, the tissues were dehydrated and mounted for imaging with a xylene-based mounting medium. H&E stained tissues were imaged on an Axio Observer Z1 Inverted Fluorescence Microscope (Zeiss).

RESULTS

IR820 dye maintains its optical properties when encapsulated in stable, monodisperse NPs

IR820-PLGA NPs were first characterized with TEM, DLS, and zeta potential measurements, which showed that they are monodisperse and spherical (Fig. 1A) with a hydrodynamic diameter of $60 \pm 10 \text{ nm}$ and a surface charge of $-40 \pm 6 \text{ mV}$. The stated synthesis conditions yielded IR820-PLGA NPs with 90% encapsulation efficiency and 18% loading capacity. The heating profile of IR820 dye free in solution or encapsulated in PLGA NPs was examined by irradiating samples diluted in PBS at $25 \mu\text{M}$ with 808 nm light for 5 min at 1.5 W/cm^2 . Thermal imaging showed that free IR820 dye and IR820-PLGA NPs heat similarly (Fig. 1B), indicating that encapsulating the dye does not alter its optical properties or its capacity to heat. Additional testing of the IR820-PLGA NPs demonstrated that their heat production is dependent upon both concentration and laser intensity (Fig. S1A and B). We further examined the optical properties and stability of IR820 dye free in solution or encapsulated in NPs by using UV-vis spectroscopy

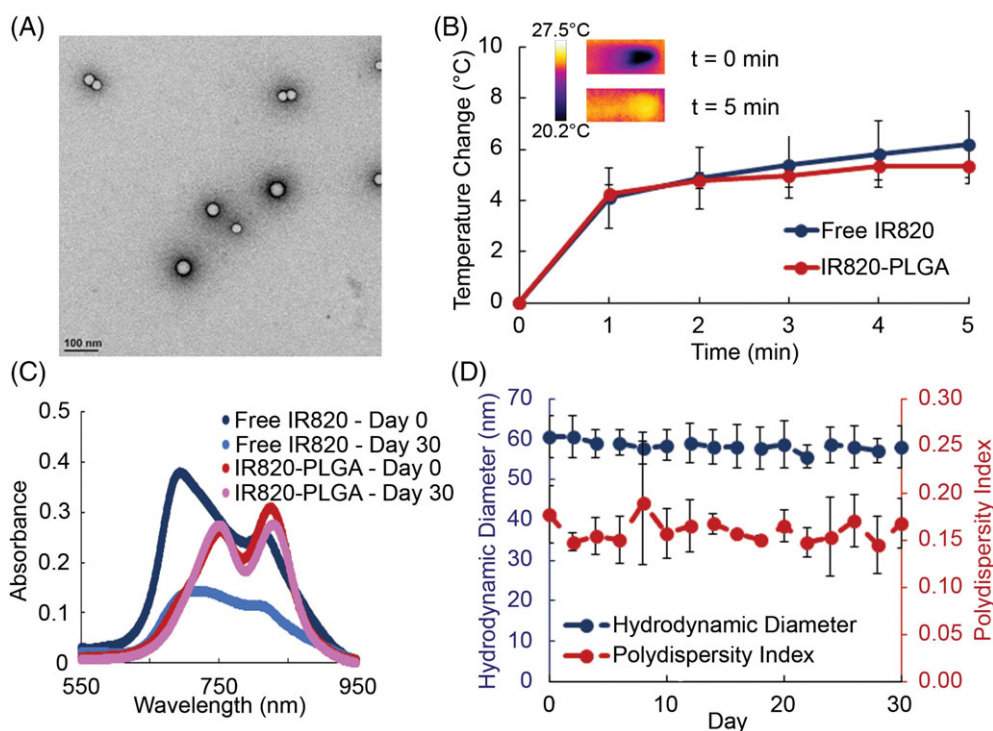


FIGURE 1. (A) TEM image showing the size and morphology of IR820-PLGA NPs. (B) The heating profile of IR820-PLGA NPs and free IR820 dye upon laser irradiation ($n = 3$). (C) The absorption profile of free IR820 and IR820-PLGA NPs before and after storage in water at 4°C for 30 days as determined by UV-vis spectrophotometry. The concentration of IR820 is $25 \mu\text{M}$ for both free and encapsulated dye. (D) The hydrodynamic diameter and polydispersity index of IR820-PLGA NPs as determined by DLS when stored in water at 4°C for 30 days ($n = 3$).

to analyze the extinction spectrum of freshly made samples and samples that had been stored in water at 4 °C for 30 days. Free IR820 dye has two characteristic extinction peaks at 810 and 685 nm that are red-shifted after encapsulation (Fig. 1C). After storage in water at 4 °C for 30 days, we observed that free IR820 dye loses its absorption capabilities, whereas IR820 encapsulated in PLGA NPs maintains its optical properties (Fig. 1C). To understand whether irradiation leading to heating impacts the optical and physical properties of the NPs, we measured their absorption spectra, hydrodynamic diameter, and polydispersity index before and after irradiation with the 808 nm laser at 1.5 W/cm² for 5 min. This revealed that IR820-PLGA NPs lose their absorption capabilities postirradiation (Fig. S1c), and this is coupled with an increase in their hydrodynamic diameter and polydispersity index (Fig. S1c and d). This suggests that IR820-PLGA NPs are best suited for application in single rounds of PTT. We also examined the stability of IR820-PLGA NPs in storage conditions using DLS. The hydrodynamic diameter and polydispersity index of the NPs were measured every 2 days for 30 days and showed no notable change throughout this time period (Fig. 1D). There was also negligible release of the IR820 dye from the IR820-PLGA NPs over a 30-day storage period after an initial burst release (Fig. S2). Altogether, these data indicate that IR820 encapsulated in PLGA NPs maintains its optical properties and these NPs are monodisperse and stable for at least 1 month in storage conditions.

IR820-PLGA NPs demonstrate time- and dose-dependent cellular binding and uptake

Next, we examined the cellular binding and uptake of free IR820 dye and IR820-PLGA NPs in MDA-MB-231 TNBC cells. We treated cells with a range of doses from 0 to 35 μM and flow cytometry showed that binding and/or uptake in cells was dose dependent for both formulations (Fig. 2A; only data for IR820-PLGA NPs are shown). We further evaluated cellular binding and uptake over a range of 8 h by treating cells with free IR820 dye and IR820-PLGA NPs at 35 μM. Flow cytometry analysis indicates that, at this dose, cellular binding and uptake of free dye and NPs is also time dependent (Fig. 2B; only data for IR820-PLGA NPs are shown). Based on these data, we chose to examine the toxicity of each treatment over the full dosing range investigated here. Additionally, we selected 4 h as the time of treatment incubation for further *in vitro* toxicity and efficacy studies because it was the time needed to achieve a log increase in uptake of the NPs.

IR820 encapsulated in PLGA NPs has less effect on metabolic activity in the absence of light activation than free IR820

We used an MTT assay to examine the relative metabolic activity of cells treated with free IR820 dye and IR820-PLGA NPs in the absence of light activation. We treated cells with each formulation at a range of doses from 0 to 35 μM for 4 h and then allowed the cells to incubate in fresh media for another 24 h. The MTT assays showed that free IR820 dye demonstrates toxicity at concentrations above 10 μM, as

indicated by cell viability of <80% (Fig. 2C). IR820-PLGA NPs, however, showed no toxicity with doses up to 35 μM (Fig. 2C). These data indicate that encapsulation of IR820 dye has less effect on metabolic activity and therefore a higher dose can be safely administered.

IR820-PLGA NPs enable proapoptotic PTT *in vitro*

We next investigated the use of IR820-PLGA NP-mediated PTT as a treatment strategy for TNBC and probed the mechanism of cell death induced by this treatment. MDA-MB-231 TNBC cells were exposed to 0 or 35 μM IR820-PLGA NPs, the maximum tolerated dose determined previously, for 4 h and then half of the samples were irradiated with an 808 nm laser. The combination of IR820-PLGA NPs and laser irradiation resulted in a significant reduction in metabolic activity 24 h posttreatment as measured by an MTT assay (Fig. 2D).

After showing that IR820-PLGA NPs can successfully induce cell death, we further evaluated the mechanism through which this occurs. As described previously, it is imperative to induce apoptosis rather than necrosis for optimal therapeutic outcomes. Thus, we assessed the mechanism of cell death by first treating cells with 0 or 10 μM IR820-PLGA NPs for 4 h and then irradiating half of the samples with 808 nm light for 5 min at 2 W/cm². After 24 h of incubation, cells were stained with Annexin V (FITC channel) and PI (PerCP channel) for analysis by flow cytometry. Cells that stain positive for Annexin V only (bottom right quadrant) are undergoing early apoptosis, cells that stain positive for Annexin V and PI (top right quadrant) are undergoing late apoptosis, and cells that stain positive for PI only (top left quadrant) are undergoing necrosis. The flow cytometric analysis showed that PTT mediated by IR820-PLGA NPs primarily induces cell death through apoptosis with no notable increase in necrotic cell percentage (Fig. 2E, representative scatter plots are shown in Figure 2F). By ANOVA with post hoc Tukey, the *p*-value for the difference in apoptosis between media and IR820-PLGA NP PTT was 0.1. These data together with the MTT data indicate that IR820-PLGA NPs can successfully mediate proapoptotic PTT of TNBC *in vitro*.

IR820-PLGA NPs maximally accumulate in tumors within 24 h

After evaluating IR820-PLGA NPs *in vitro*, we then examined their ability to mediate PTT of TNBC *in vivo* using a subcutaneous murine xenograft model. First, we investigated the tumor accumulation and biodistribution of these particles after intravenous injection. The tumor accumulation studies, which monitored IR820 signal in the tumors with an IVIS system over a period of 4 days postinjection, indicated that IR820-PLGA NPs maximally accumulate in tumors at or before 24 h (Fig. 3A). We examined the distribution of the IR820 signal in mice exposed to IR820-PLGA NPs at 24-h postinjection by excising the major organs (liver, brain, heart, lungs, kidneys, and spleen) and tumors for *ex vivo* fluorescence imaging. In addition to prominent accumulation of IR820 in the tumors, we also found IR820 signal in the liver, lungs, and kidneys (Fig. 3B). Overall, these data mark

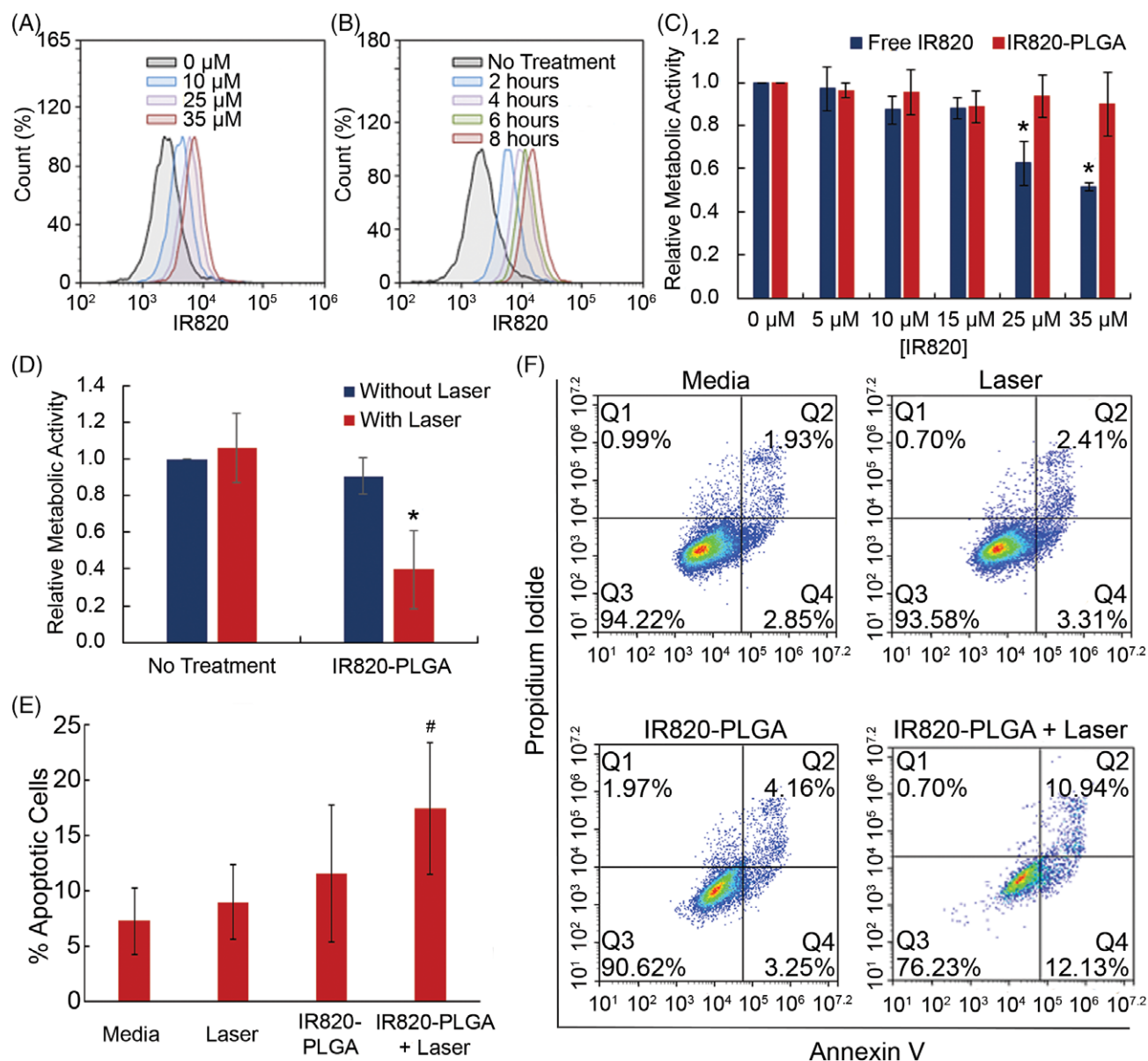


FIGURE 2. Flow cytometric analysis of the cellular binding and uptake of IR820-PLGA NPs based on (A) dose and (B) time of incubation. (C) Relative metabolic activity of MDA-MB-231 TNBC cells exposed to free IR820 dye or IR820-PLGA NPs without light exposure. $*p < 0.05$ (D) Relative metabolic activity of MDA-MB-231 cells that received PTT mediated by IR820-PLGA NPs (35 μM) and laser irradiation versus control cells that were exposed to only saline, only IR820-PLGA NPs (35 μM), or saline and laser irradiation. $*p < 0.05$ versus untreated control by ANOVA with post hoc Tukey. (E) The percentage of apoptotic cells in MDA-MB-231 samples that were exposed to no treatment, laser only, IR820-PLGA NPs only (10 μM), or PTT (IR820-PLGA NPs + laser; 10 μM). $\#p = 0.1$ versus untreated control by ANOVA with post hoc Tukey. (F) Representative scatterplots demonstrating the fraction of MDA-MB-231 cells in early apoptosis (bottom right quadrant), late apoptosis (top right quadrant), or necrosis (top left quadrant) following treatment with media only, laser only, IR820-PLGA NPs only, or PTT (IR820-PLGA NPs + laser). Red color indicates a high density of cells and blue color indicates a low density of cells.

the optimal timing for laser irradiation after intravenous injection as 24 h postdelivery.

PTT mediated by IR820-PLGA NPs provides sufficient heating of tumors

Next, we evaluated the ability of free IR820 dye and IR820-PLGA NPs to enable tumor heating during irradiation with NIR light by thermal camera imaging. We injected saline,

free IR820 dye, or IR820-PLGA NPs through the tail vein of tumor-bearing mice and let the treatments circulate for 24 h. The tumors were then irradiated with an 810 nm laser for 5 min and the temperature was monitored with a thermal camera. While free IR820 dye provided mild and unsustainable heating over the 5 min irradiation period, IR820-PLGA NPs produced sustained heating above 42 $^{\circ}\text{C}$, the threshold considered sufficient for PTT under the conditions in this study (Fig. 3C).⁵⁴

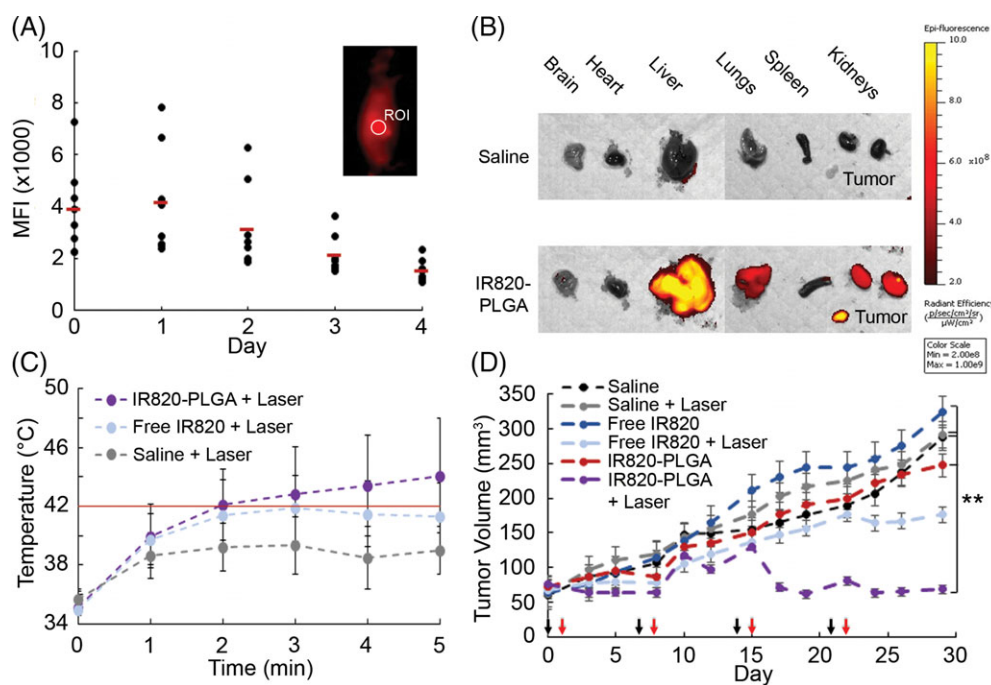


FIGURE 3. (A) Mean fluorescence intensity (MFI) of IR820 in tumors of mice at different times post-intravenous injection of IR820-PLGA NPs. The inset displays a representative image of IR820-PLGA NP fluorescence at 24 h after injection and the region of interest (ROI) in which the fluorescence intensity was measured. (B) *Ex vivo* analysis of IR820 signal in the brain, heart, liver, lungs, spleen, kidneys, and tumors of mice 24 h after they received intravenous injections of IR820-PLGA NPs or saline. (C) Mean tumor temperature in mice treated with saline, free IR820, or IR820-PLGA NPs during laser irradiation. These temperatures were recorded during the first of four treatment cycles. The red line at 42°C indicates the threshold considered sufficient to induce PTT under the conditions in this study. (D) Tumor volume versus time in mice exposed to PTT mediated by IR820-PLGA NPs or various control treatments ($n = 8$ for all groups except saline + laser, for which $n = 7$). All treatments were injected intravenously at an IR820 concentration of $350\ \mu\text{M}$. Mice whose tumors received laser exposure were irradiated at $1.5\ \text{W}/\text{cm}^2$ for 5 min. Black arrows indicate the days of treatment injections (days 0, 7, 14, and 21) and red arrows indicate the days of laser irradiation (days 1, 8, 15, and 22). ** $p < 0.01$.

PTT with IR820-PLGA NPs significantly reduces TNBC tumor growth

We then investigated whether PTT mediated by IR820-PLGA NPs could reduce tumor growth in our subcutaneous xenograft model. The mice were divided into six treatment groups: saline \pm irradiation, free IR820 dye \pm irradiation, and IR820-PLGA NPs \pm irradiation. Throughout a 30-day treatment period, the mice were injected with the treatments and irradiated four times (days indicated by black and red arrows, respectively, in Fig. 3D), and tumor volume was measured three times per week. The mean tumor volume within each treatment group is shown in Figure 3d and the individual tumor growth curves and final tumor size for each mouse are shown in Figure S3. Mice treated with free IR820 dye and irradiated with the laser showed a slight reduction in tumor volume at the end of the treatment period (Fig. 3D, Fig. S3). By comparison, mice treated with IR820-PLGA NPs and irradiated with the laser experienced a substantial and statistically significant reduction in tumor growth, and two mice even exhibited complete regression (Fig. 3D, Fig. S3). Finally, we evaluated the impact of each treatment on the morphology of major organs and tumors using H&E staining. Only the tumors treated with IR820-PLGA NPs and irradiated with the laser demonstrated any notable changes in tissue morphology, indicative of the effects of PTT (Fig. S4). Together, these data confirm that the effects of PTT are

confined to TNBC tumors where both IR820-PLGA NPs and light are applied.

DISCUSSION

PTT has shown promise as an alternative strategy for TNBC therapy,^{4-7,9} and here we aimed to expand this potential by creating a biodegradable NP platform that enables proapoptotic PTT. The key advantage of PTT relative to other therapies is its high precision, as the use of tissue-penetrating NIR light as an activating source means that heat is produced only where this light and photoresponsive NPs are combined within tumors. In addition, PTT is minimally invasive, has negligible morbidity, and is less susceptible to cellular resistance than other treatments because it induces cell death primarily through physical, rather than biochemical, mechanisms. In the past, PTT has most commonly been mediated by gold-based NPs.^{10,29-32} However, these formulations have unknown long-term health effects and typically result in rapid and very high heating that leads to cellular necrosis. Necrosis has been shown to yield a pro-inflammatory immune response, which can promote tumor recurrence if PTT is not combined with an appropriate immunotherapy regimen.^{8,17,18} Thus, it is imperative that PTT regimens intended for use as a monotherapy be designed to induce apoptosis, which can yield an anti-inflammatory immune response and promote long-term

remission. While it is possible to tune the parameters of PTT mediated by gold-based NPs to primarily induce apoptosis, for example, by lowering the intensity of the incident light, these types of NPs will still remain in the body for extended periods of time with unknown long-term consequences. Several researchers have developed biodegradable, NIR-absorbing NPs to address the safety concerns associated with gold-based NPs,^{21,37–45,48,49,51} but they have not fully evaluated whether the mechanism of cell death induced by PTT with these NPs is primarily apoptotic or necrotic. In this work, we developed biodegradable NPs loaded with IR820 dye, and demonstrated that they enable proapoptotic PTT of TNBC. Further, we showed that PTT mediated by these NPs could induce tumor regression *in vivo*. Thus, with this formulation, we not only address the potential health concern related to gold-based NPs currently used for PTT, but also provide a potent new platform for proapoptotic PTT of TNBC.

To evaluate PTT mediated by IR820-PLGA NPs as a proapoptotic strategy for TNBC therapy, we examined the optical properties and stability of these NPs, their ability to enter cells, their toxicity without light exposure, and their effect on cell viability after irradiation. Our results show that these NPs are stable for 1 month in storage conditions and that IR820 maintains its optical properties when encapsulated in PLGA (Fig. 1). Encapsulation also decreases the toxicity of the dye, which amplifies the dose that can be safely administered for more potent mediation of PTT (Fig. 2). We also demonstrated that these NPs can bind and enter MDA-MB-231 cells, as IR820 signal is detectable at significant quantities in and/or on MDA-MB-231 cells over an 8-h period following NP addition to cell culture (Fig. 2), but we have not probed the mechanism by which IR820-PLGA NPs might enter these cells. Literature has shown that polymeric micelles can deliver hydrophobic cargo to other cell types through membrane-mediated transport, likely facilitated by poly(ethylene glycol)-induced fusion with the cell membrane.⁵⁵ The uptake of NPs composed strictly of PLGA has also been investigated in various cell types, indicating uptake occurs by an endocytic process.^{56,57} Future studies should evaluate the mechanism by which IR820-PLGA NPs enter MDA-MB-231 and other TNBC cells using inhibitors of various endocytic pathways to corroborate these prior findings and the results presented here.

In further *in vitro* studies, we demonstrated that PTT mediated by IR820-PLGA NPs primarily induces apoptosis (Fig. 2), which is vastly preferred over necrosis when PTT is used as a standalone therapy. The treatment conditions used in our analysis of cellular apoptosis versus necrosis likely contributed to the proapoptotic results, as we previously noted that the ability to induce apoptosis versus necrosis depends on a variety of factors, including irradiation time, irradiation intensity, NP concentration, and more.⁸ Here, we demonstrate that the heating profile of IR820-PLGA NPs is dependent upon both concentration and laser intensity (Fig. S1). Thus, we posit that performing these experiments at elevated concentrations and/or laser intensities would increase the relative fraction of cells undergoing necrosis versus apoptosis, though this would have to be evaluated through further experimentation.

We also examined the ability of IR820-PLGA NPs to mediate PTT *in vivo* using mice bearing subcutaneous TNBC xenografts by investigating their biodistribution, studying their ability to heat tumors upon light exposure resulting in tumor regression, and examining their impact on off-target organs. Our results demonstrate that IR820-PLGA NPs maximally accumulate in tumors within 24 h after intravenous injection (Fig. 3). At this time point, we found notable IR820 signal in the liver, lungs, and kidneys, in addition to significant accumulation in the tumor. Given the size of our NPs, we posit that the IR820 signal in the liver is due to clearance by the mononuclear phagocytic system, and the signal in the kidneys is likely free IR820 dye released from the NPs. While our observation that IR820-PLGA NPs accumulate in tumors to a greater extent at 24 h than at later time points is consistent with our previous experience using other NPs,^{14,15} in this study we did not examine time points prior to 24 h. Future studies should examine the biodistribution and tumor accumulation of IR820-PLGA NPs at earlier time points, as these studies may reveal a more optimal time to perform the laser irradiation.

Our results also showed that IR820-PLGA NPs produce sufficient heat during tumor irradiation to significantly slow the growth of subcutaneous MDA-MB-231 tumors, with some mice even experiencing complete remission (Fig. 3, Fig. S3). The administered dose of IR820 used in these studies (100 μ L at 350 μ M) was selected based on prior literature reports using intravenously injected NIR absorbing dyes.^{6,21,51,53} Traditionally, PTT is only administered once, but in this study, we performed four rounds of treatment (one per week). The reason for this is that we were operating under NP dose and laser irradiation conditions that would induce mild tumor heating, rather than high tumor heating, and we expected that this approach would require more than one round of treatment to induce tumor regression. Indeed, after the third round of treatment, we began to observe substantial differences in tumor growth between the IR820-PLGA NP PTT group and the other treatment groups. In the future, the NP dose, laser irradiation conditions, and time of laser irradiation post-NP injection should be altered to determine whether effective tumor regression can be achieved with only a single round of treatment. In addition, future studies should investigate whether PTT mediated by IR820-PLGA NPs is effective against other models of TNBC. Here, we used human MDA-MB-231 cells implanted subcutaneously in nude mice, but several other TNBC models exist that may more accurately reflect the aggressive nature of human TNBC.^{58–60} For example, studies could be performed using tumors implanted orthotopically in the mammary fat pad, or using murine 4T1 cells that grow in immune-competent mice and can spontaneously metastasize to distant sites after implantation. Since PTT can induce an antitumor immune response, performing studies in immune competent animals could more thoroughly reveal the potential impact of this treatment. Further, the use of humanized patient-derived xenograft TNBC models that are responsive to immunotherapy could allow for analysis of this strategy in combination with immunotherapy. Overall,

demonstrating the effectiveness of this treatment in several animal models will validate its potential as an anti-TNBC therapy.

Finally, we demonstrated that only tumors that were exposed to both IR820-PLGA NPs and light showed notable changes in tissue morphology, consistent with the effects and high precision of PTT (Fig. S4). Given that these NPs are biodegradable and the IR820 (which is cytotoxic on its own in high concentrations) will be released over time, future studies should investigate the long-term effects of the released IR820 on the organs in which the IR820-PLGA NPs accumulate. Based on the degradation profile of PLGA in physiological conditions,⁶¹ we anticipate that the amount of released IR820 present in various tissues would not surpass cytotoxic thresholds. However, future safety studies need to be performed in order to validate the compatibility of this platform and determine the maximum tolerated dose. These should be performed using immune competent animals, as this would most accurately reflect the body's response to the NPs and released IR820.

CONCLUSION

In summary, we present IR820-loaded PLGA NPs as new, biodegradable, potent mediators of PTT for the treatment of TNBC. These NPs overcome the limitations of other established PTT mediators in that they are biodegradable and enable cell death through apoptosis. Future work should directly compare these IR820-PLGA NPs to traditional gold-based PTT agents for a quantitative analysis of the differences seen in each treatment. Additionally, future studies will need to be performed to validate that the mechanism of cell death triggered by PTT with these NPs *in vivo* is also apoptotic, as our studies only confirmed this to be the case *in vitro*. Additionally, future studies should examine the antitumor potency and long-term safety of this nanoformulation using mice with an intact immune system, as this will reveal the full therapeutic potential of this formulation. Overall, our work lays the foundation for successful use of these IR820-PLGA NPs to enable proapoptotic PTT of TNBC and other solid cancer tumors.

ACKNOWLEDGMENTS

This research was supported by the National Institute of General Medical Sciences (NIGMS) of the National Institutes of Health (NIH) under Award Number R35GM119659. Microscopy access was supported by grants from the NIH-NIGMS (P20 GM103446), the National Science Foundation (IIA-1301765), and the State of Delaware. The content is solely the responsibility of the authors and does not necessarily represent the official views of the funding agencies.

REFERENCES

1. Bianchini G, Balko JM, Mayer IA, Sanders ME, Gianni L. Triple-negative breast cancer: Challenges and opportunities of a heterogeneous disease. *Nature* 2016;13:674–690.
2. Turner N, Moretti E, Siclari O, Migliaccio I, Santarpia L, D'Incalci M, Piccolo S, Veronesi A, Zambelli A, Del Sal G, Di Leo A. Targeting triple negative breast cancer: Is p53 the answer? *Cancer Treat Rev* 2013;39:541–550.
3. Griffiths CL, Olin JL. Triple negative breast cancer: A brief review of its characteristics and treatment options. *J Pharm Pract* 2012;25(3): 319–323.
4. Su S, Ding Y, Li Y, Wu Y, Nie G. Integration of photothermal therapy and synergistic chemotherapy by a porphyrin self-assembled micelle confers chemosensitivity in triple-negative breast cancer. *Biomaterials* 2016;80:169–178.
5. Ayala-Orozco C, Urban C, Bishnoi S, Urban A, Charron H, Mitchell T, Shea M, Nanda S, Schiff R, Halas N, Joshi A. Sub-100 nm gold nanomatryoshkas improve photo-thermal therapy efficacy in large and highly aggressive triple negative breast tumors. *J Control Release* 2014;191:90–97.
6. Su S, Tian Y, Li Y, Ding Y, Ji T, Wu M, Wu Y, Nie G. “Triple-punch” strategy for triple negative breast cancer therapy with minimized drug dosage and improved antitumor efficacy. *ACS Nano* 2015;9(2): 1367–1378.
7. Yang Z, Liu T, Xie Y, Sun Z, Liu H, Lin J, Liu C, Mao Z-W, Nie S. Chitosan layered gold nanorods as synergistic therapeutics for photothermal ablation and gene silencing in triple-negative breast cancer. *Acta Biomater* 2015;25:194–204.
8. Melamed JR, Edelstein RS, Day ES. Elucidating the fundamental mechanisms of cell death triggered by photothermal therapy. *ACS Nano* 2015;9(1):6–11.
9. Fay BL, Melamed JR, Day ES. Nanoshell-mediated photothermal therapy can enhance chemotherapy in inflammatory breast cancer cells. *Int J Nanomed* 2015;10:6931–6941.
10. Riley RS, Day ES. Gold nanoparticle-mediated photothermal therapy: Applications and opportunities for multimodal cancer treatment. *Wiley Interdiscip Rev Nanomed Nanobiotechnol* 2017;9(4):e1449.
11. Matsumura Y, Maeda H. A new concept for macromolecular therapeutics in cancer chemotherapy: Mechanism of tumoritropic accumulation of proteins and the antitumor agent Smancs. *Cancer Res* 1986;46:6387–6392.
12. Maeda H. The enhanced permeability and retention (EPR) effect in tumor vasculature: The key role of tumor-selective macromolecular drug targeting. *Adv Enzyme Regul* 2001;41:189–207.
13. Hussein EA, Zagho MM, Nasrallah GK, Elzatahry AA. Recent advances in functional nanostructures as cancer photothermal therapy. *Int J Nanomed* 2018;13:2897–2906.
14. Day ES, Thompson PA, Zhang L, Lewinski NA, Ahmed N, Drezek RA, Blaney SM, West JL. Nanoshell-mediated photothermal therapy improves survival in a murine glioma model. *J Neurooncol* 2011;104(1):55–63.
15. Day ES, Zhang L, Thompson PA, Zawaski JA, Kaffes CC, Gaber MW, Blaney SM, West JL. Vascular-targeted photothermal therapy of an orthotopic murine glioma model. *Nanomedicine* 2012;7(8):1133–1148.
16. Weissleder R. A clearer vision for *in vivo* imaging. *Nat Biotechnol* 2001;19:316–317.
17. Pérez-Hernández M, Del Pino P, Mitchell SG, Moros M, Stepien G, Pelaz B, Parak WJ, Gálvez EM, Pardo J, de la Fuente JM. Dissecting the molecular mechanism of apoptosis during photothermal therapy using gold nanoprisms. *ACS Nano* 2015;9(1):52–61.
18. Bear AS, Kennedy LC, Young JK, Perna SK, Almeida JPM, Lin AY, Eckels PC, Drezek RA, Foster AE. Elimination of metastatic melanoma using gold Nanoshell-enabled Photothermal therapy and adoptive T cell transfer. *PLoS One* 2013;8(7):e69073.
19. Sweeney EE, Cano-Mejia J, Fernandes R. Photothermal therapy generates a thermal window of immunogenic cell death in neuroblastoma. *Small* 2018;14:1800678.
20. Martin S, Henry CM, Cullen SP. A perspective on mammalian caspases as positive and negative regulators of inflammation. *Mol Cell* 2012;46:387–397.
21. Chen Q, Xu L, Liang C, Wang C, Peng R, Liu Z. Photothermal therapy with immune-adjuvant nanoparticles together with checkpoint blockade for effective cancer immunotherapy. *Nat Commun* 2016;7:713193.
22. Sauter B, Albert ML, Francisco L, Larsson M, Somersan S, Bhardwaj N. Consequences of cell death: Exposure to necrotic tumor cells, but not primary tissue cells or apoptotic cells, induces the maturation of immunostimulatory dendritic cells. *J Exp Med* 2000;191(3):423–433.
23. Pattani VP, Shah J, Atalis A, Sharma A, Tunnell JW. Role of apoptosis and necrosis in cell death induced by nanoparticle-mediated photothermal therapy. *J Nanopart Res* 2015;17:20.

24. Sweeney EE, Burga RA, Li C, Zhu Y, Fernandes R. Photothermal therapy improves the efficacy of a MEK inhibitor in neurofibromatosis type 1-associated malignant peripheral nerve sheath tumors. *Sci Rep* 2016;6:37035.
25. Mocan T, Matea CT, Cojocaru I, Ilie I, Tabaran FA, Zaharie F, Iancu C, Bartos D, Mocan L. Photothermal treatment of human pancreatic cancer using PEGylated multi-walled carbon nanotubes induces apoptosis by triggering mitochondrial membrane depolarization mechanism. *J Cancer* 2014;5(8):679–688.
26. Tong L, Cheng J-X. Gold nanorod-mediated photothermolysis induces apoptosis of macrophages via damage of mitochondria. *Nanomedicine* 2009;4(3):265–276.
27. Li J-L, Gu M. Surface plasmonic gold nanorods for enhanced two-photon microscopic imaging and apoptosis induction of cancer cells. *Biomaterials* 2010;31:9492–9498.
28. Dai Q, Wilhelm S, Ding D, Syed AM, Sindhvani S, Zhang Y, Chen YY, MacMillan P, Chan WCW. Quantifying the ligand-coated nanoparticle delivery to cancer cells in solid tumors. *ACS Nano* 2018;12:8423–8435.
29. Stone J, Jackson S, Wright D. Biological applications of gold nanorods. *Wiley Interdiscip Rev Nanomed Nanobiotechnol* 2011;3:100–109.
30. Skrabalak SE, Chen J, Au L, Lu X, Li X, Xia Y. Gold nanocages for biomedical applications. *Adv Mater* 2007;19(20):3177–3184.
31. Dam DHM, Culver KSB, Kandela I, Lee RC, Chandra K, Lee H, Mantis C, Ugolkov A, Mazar AP, Odom TW. Biodistribution and *in vivo* toxicity of aptamer-loaded gold nanostars. *Nanomedicine* 2015;11(3):671–679.
32. Cole JR, Mirin NA, Knight MW, Goodrich GP, Halas NJ. Photothermal efficiencies of nanoshells and nanorods for clinical therapeutic applications. *J Phys Chem C* 2009;113:12090–12094.
33. Stern JM, Kibanov Solomonov VV, Sazykina E, Schwartz JA, Gad SC, Goodrich GP. Initial evaluation of the safety of nanoshell-directed photothermal therapy in the treatment of prostate disease. *Int J Toxicol* 2015;35(1):38–46.
34. Nanospectra Biosciences, Inc. Efficacy Study of AuroLase Therapy in Subjects With Primary and/or Metastatic Lung Tumors. Available online: <https://clinicaltrials.gov/ct2/show/NCT01679470?term=auroshell&rank=3> (accessed on September 30, 2018).
35. Nanospectra Biosciences, Inc. Pilot Study of AuroLase™ Therapy in Refractory and/or Recurrent Tumors of the Head and Neck. Available online: <https://clinicaltrials.gov/ct2/show/NCT00848042?term=auroshell&rank=2> (accessed on September 30, 2018).
36. Song X, Chen Q, Liu Z. Recent advances in the development of organic photothermal nano-agents. *Nano Res* 2015;8(2):340–354.
37. Yue C, Liu P, Zheng M, Zhao P, Wang Y, Ma Y, Cai L. IR-780 dye loaded tumor targeting theranostic nanoparticles for NIR imaging and photothermal therapy. *Biomaterials* 2013;34:6853–6861.
38. Chen Y, Li Z, Wang H, Wang Y, Han H, Jin Q, Ji J. IR-780 loaded phospholipid mimicking homopolymeric micelles for near-IR imaging and photothermal therapy of pancreatic cancer. *ACS Appl Mater Interfaces* 2016;8:6852–6858.
39. Wang K, Zhang Y, Wang J, Yuan A, Sun M, Wu J, Hu Y. Self-assembled IR780-loaded transferrin nanoparticles as an imaging, targeting and PDT/PTT agent for cancer therapy. *Sci Rep* 2016;6:27421.
40. Kuang Y, Zhang K, Cao Y, Chen X, Wang K, Liu M, Pei R. Hydrophobic IR-780 dye encapsulated in cRGD-conjugated solid lipid nanoparticles for NIR imaging-guided photothermal therapy. *ACS Appl Mater Interfaces* 2017;9:12217–12226.
41. Yuan A, Qui X, Tang X, Liu W, Wu J, Hu Y. Self-assembled PEG-IR-780-C13 micelle as a targeting, safe and highly-effective photothermal agent for *in vivo* imaging and cancer therapy. *Biomaterials* 2015;51:184–193.
42. Chen Q, Wang C, Zhan Z, He W, Cheng Z, Li Y, Liu Z. Near-infrared dye bound albumin with separated imaging and therapy wavelength channels for imaging-guided photothermal therapy. *Biomaterials* 2014;35:8206–8214.
43. Zheng M, Zhao P, Luo Z, Gong P, Zheng C, Zhang P, Yue C, Gao D, Ma Y, Cai L. Robust ICG theranostic nanoparticles for folate targeted cancer imaging and highly effective photothermal therapy. *ACS Appl Mater Interfaces* 2014;6:6709–6716.
44. Zheng X, Xing D, Zhou F, Wu B, Chen WR. Indocyanine green-containing nanostructure as near infrared dual-functional targeting probes for optical imaging and photothermal therapy. *Mol Pharm* 2011;8:447–456.
45. Liu P, Yue C, Shi B, Gao G, Li M, Wang B, Ma Y, Cai L. Dextran based sensitive theranostic nanoparticles for near-infrared imaging and photothermal therapy *in vitro*. *Chem Commun* 2013;49:6143–6145.
46. Peng CL, Shih YH, Lee PC, Hsieh TMH, Luo TY, Shieh MJ. Multimodal image-guided photothermal therapy mediated by ¹⁸⁸Re-labeled micelles containing a cyanine-type photosensitizer. *ACS Nano* 2011;5(7):5594–5607.
47. Lovell JF, Jin CS, Huynh E, Jin H, Kim C, Rubinstein JL, Chan WCW, Cao W, Wang LV, Zheng G. Porphyrin nanovesicles generated by porphyrin bilayers for use as multimodal biophotonic contrast agents. *Nat Mater* 2011;10:324–332.
48. Kumar P, Srivastava R. IR 820 dye encapsulated in polycaprolactone glycol chitosan: Poloxamer blend nanoparticles for photo immunotherapy for breast cancer. *Mater Sci Eng C* 2015;57:321–327.
49. Li W, Peng J, Tan L, Wu J, Shi K, Qu Y, Wei X, Qian Z. Mild photothermal therapy/photodynamic therapy/chemotherapy of breast cancer by Lyp-1 modified docetaxel/IR820 co-loaded micelles. *Biomaterials* 2016;106:119–133.
50. Valcourt DM, Harris J, Riley RS, Dang M, Wang J, Day ES. Advances in targeted nanotherapeutics: From bioconjugation to biomimicry. *Nano Res* 2018;11(10):4999–5016.
51. Zheng M, Yue C, Ma Y, Gong P, Zhao P, Zheng C, Sheng Z, Zhang P, Wang Z, Cai L. Single-step assembly of DOX/ICG loaded lipid-polymer nanoparticles for highly effective chemo-photothermal combination therapy. *ACS Nano* 2013;7(3):2056–2067.
52. Srinivasan S, Manchanda R, Lei T, Nagesetti A, Fernandez-Fernandez A, McGoron AJ. Targeted nanoparticles for simultaneous delivery of chemotherapeutic and hyperthermia agents—An *in vitro* study. *J Photochem Photobiol B* 2014;136:81–90.
53. Zhao P, Zheng M, Yue C, Luo Z, Gong P, Gao G, Sheng Z, Zheng C, Cai L. Improving drug accumulation and photothermal efficacy in tumor depending on size of ICG loaded lipid-polymer nanoparticles. *Biomaterials* 2014;35:6037–6046.
54. Wu F. Biological effects of thermal ablation on tumor. In: Moros EG, editor. *Physics of Thermal Therapy: Fundamentals and Clinical Applications*. Boca Raton, FL: Taylor & Francis Group; 2012. p 257–259.
55. Chen H, Kim S, Li L, Wang S, Park K, Cheng JX. Release of hydrophobic molecules from polymer micelles into cell membranes revealed by Förster resonance energy transfer imaging. *PNAS* 2008;105(18):6596–6601.
56. Qaddoumi MG, Ueda H, Yang J, Davda J, Labhasetwar V, Lee VHL. The characteristics and mechanisms of uptake of PLGA nanoparticles in rabbit conjunctival epithelial cell layers. *Pharm Res* 2003;21(4):641–648.
57. Cartiera MS, Johnson KM, Rajendran V, Caplan MJ, Saltzman WM. The uptake and intracellular fate of PLGA nanoparticles in epithelial cells. *Biomaterials* 2009;30(14):2790–2798.
58. Holen I, Speirs V, Morrissey B, Blyth K. *In vivo* models in breast cancer research: Progress, challenges and future directions. *Dis Model Mech* 2017;10:359–371.
59. Ghosh A, Sarkar S, Banerjee S, Behbod F, Tawfik O, McGregor D, Graff S, Banerjee SK. MIND model for triple-negative breast cancer in syngeneic mice for quick and sequential progression analysis of lung metastasis. *PLoS One* 2018;13(5):e0198143.
60. Kaur P, Nagaraja GM, Zheng H, Gizachew D, Galukande M, Krishnan S, Asea A. A mouse model for triple-negative breast cancer tumor-initiating cells (TNBC-TICs) exhibits similar aggressive phenotype to the human disease. *BMC Cancer* 2012;12:120.
61. Makadia HK, Siegel SJ. Poly lactic-co-glycolic acid (PLGA) as biodegradable controlled drug delivery carrier. *Polymers (Basel)* 2011;3(3):1377–1397.